

Midbrain circuits that set locomotor speed and gait selection

V. Caggiano^{1†*}, R. Leiras^{1,2*}, H. Goñi-Errro^{1,2}, D. Masini³, C. Bellardita^{1,2}, J. Bouvier^{1†}, V. Caldeira¹, G. Fisone³ & O. Kiehn^{1,2}

Locomotion is a fundamental motor function common to the animal kingdom. It is implemented episodically and adapted to behavioural needs, including exploration, which requires slow locomotion, and escape behaviour, which necessitates faster speeds. The control of these functions originates in brainstem structures, although the neuronal substrate(s) that support them have not yet been elucidated. Here we show in mice that speed and gait selection are controlled by glutamatergic excitatory neurons (GlutNs) segregated in two distinct midbrain nuclei: the cuneiform nucleus (CnF) and the pedunculopontine nucleus (PPN). GlutNs in both of these regions contribute to the control of slower, alternating-gait locomotion, whereas only GlutNs in the CnF are able to elicit high-speed, synchronous-gait locomotion. Additionally, both the activation dynamics and the input and output connectivity matrices of GlutNs in the PPN and the CnF support explorative and escape locomotion, respectively. Our results identify two regions in the midbrain that act in conjunction to select context-dependent locomotor behaviours.

Activities such as exploring the surroundings, searching for food or escaping from danger depend on locomotor movements. The episodic nature of locomotion requires cycles of initiation and termination. In addition, during locomotion and depending on behavioural demands, changes of speed are necessary. In quadrupeds this function is often associated with changes in limb coordination, resulting in different gaits¹. In mice, the alternating gaits—walk and trot—are associated with slow locomotor speeds, whereas the synchronous gaits—gallop and bound—involve fast locomotor speeds¹ and are mostly used during escape-like behaviour. The executive locomotor circuits that control the coordination of muscle activity are localized in the spinal cord^{2–6}, however the commands for initiation and gait selection may originate in different supraspinal structures. The most important neuronal structure that has been implicated in these functions is the mesencephalic locomotor region (MLR)^{7–9}, which is located in the midbrain.

The MLR was first defined functionally in cats as a region localized in or around the CnF, in which continuous electrical stimulation evoked persistent locomotion¹⁰. Analogues of the MLR have been observed in many vertebrates—including fish, rodents, primates and humans^{8,9,11,12}—but with conflicting results as to their anatomical location. In addition to the CnF, the more ventrally located PPN has also been implicated in locomotor control. Besides being anatomically separated, each of these regions contain neurons with diverse transmitter phenotypes with excitatory long-range projection neurons—glutamatergic in the CnF and both glutamatergic and cholinergic in the PPN—intermingled with local inhibitory interneurons^{11,12}. Electrical stimulation or lesion studies are therefore unable to distinguish the contribution from the various intermingled neuronal populations present in these areas^{12,13}. Recently, optogenetic manipulations have shown that stimulation of GlutNs in and around the PPN induces locomotion in mice¹⁴. The MLR has thus been previously regarded as a single entity, precluding any evaluation of the putative divergent control of locomotion by subpopulations of neurons in the CnF and the PPN. As such, the question of whether—and if so, how—neuronal

populations of the CnF and the PPN control locomotion remains unanswered.

Here we address this question by using cell-type-specific targeting to modulate and record the activity of neurotransmitter-defined neurons in either the CnF or the PPN. Our results reveal that the MLR is defined by glutamatergic subpopulations of neurons in both the PPN and the CnF that may act in conjunction to control slower, alternating-gait locomotion. Furthermore, glutamatergic neurons in the PPN promote locomotion for the purpose of explorative behaviour, whereas those in the CnF promote escape locomotion. Our study identifies circuits that have key roles in the appropriate command pathways for selecting locomotor outputs contingent on behavioural contexts.

Control of speed by CnF and PPN cells

The anatomical locations of the CnF and the PPN are shown in Fig. 1a, b. The glutamatergic cells in the CnF and the PPN express the vesicular glutamate transporter 2, Vglut2 (Allen Brain Atlas and ref. 15) (Fig. 1c). Therefore, to target glutamatergic neurons in the CnF or the PPN, we injected a Cre-dependent adeno-associated virus (AAV) carrying channelrhodopsin-2 (ChR2) and the fluorescent tags mCherry or enhanced yellow fluorescent protein (eYFP) (denoted AAV-DIO-ChR2-eYFP/mCherry) into *Vglut2^{cre}* mice (ref. 16, Fig. 1d, f; injection sites in Extended Data Fig. 1a, b).

In a linear corridor¹, unilateral light activation of Vglut2⁺ChR2 CnF neurons led to the initiation of full-body locomotion in resting mice ($N = 9$ out of 9 mice; locomotor movements detected in 115 out of 131 trials, 88%). Increasing the stimulation frequencies stepwise from threshold values of around 2–5 Hz to maximum frequencies at 50 Hz progressively increased the speed of locomotion ($P < 0.05$, Kruskal–Wallis test, post hoc analysis with Bonferroni correction for multiple comparisons; between speeds at different frequencies shown in Fig. 1e, h, blue line and Extended Data Fig. 2a; $P < 0.001$, Spearman correlation $r = 0.32$ between frequency of stimulation and maximum speed, Supplementary Video 1). The activation of Vglut2⁺ChR2

¹Mammalian Locomotor Laboratory, Department of Neuroscience, Karolinska Institutet, 17177 Stockholm, Sweden. ²Department of Neuroscience, University of Copenhagen, Blegdamsvej 3, 2200 Copenhagen, Denmark. ³Laboratory of Molecular Neuropharmacology, Department of Neuroscience, Karolinska Institutet, 17177 Stockholm, Sweden. †Present addresses: Computational Biology Center, IBM T.J. Watson Research Center, 1101 Kitchawan Road, Route 134, Yorktown Heights, New York 10598, USA (V.Cag.); Paris-Saclay Institute of Neuroscience, UMR9197, CNRS and Université Paris-11, 91190 Gif-sur-Yvette, France (J.B.).

*These authors contributed equally to this work.

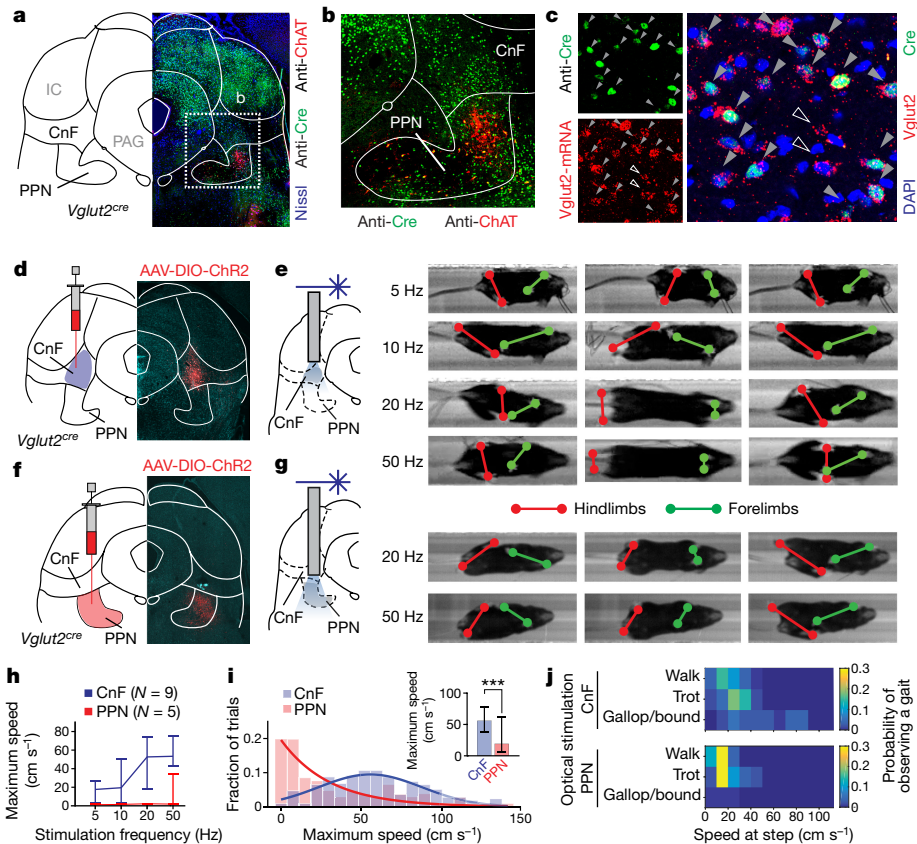


Figure 1 | The control of speed and gait by glutamatergic neurons in the CnF and the PPN. **a–c.** Identification of regions in *Vglut2^{Cre}* mice and localization of neurotransmitters. ChAT, choline acetyltransferase; DAPI, 4',6-diamidino-2-phenylindole; IC, inferior colliculus; PAG, periaqueductal grey. Solid arrowheads in **c** show *Vglut2⁺* cells. **d–g.** Examples of locomotion induced by optical stimulation of the CnF (**d, e**) and the PPN (**f, g**).

CnF neurons produced a wide range of speeds (Fig. 1i, blue) and all gaits: the alternating gaits of walk and trot and the synchronous gaits of gallop and bound (Fig. 1e, j, top)^{1,17,18}. The onset of locomotion was in the range of 100 to 150 ms (Extended Data Fig. 2c, blue line) and remained constant with the variation of stimulation frequency ($P > 0.05$, Kruskal–Wallis test).

Light activation of the *Vglut2⁺ChR2* PPN neurons also initiated locomotion from rest (Fig. 1f, g, $N = 5$ out of 7 mice; movements detected in 31 out of 67 trials, 46%). Low-frequency stimulation (<10 Hz) was not able to induce locomotion (Fig. 1h; Extended Data Fig. 2b). Increasing the frequency of stimulation increased the speed of locomotion ($P > 0.05$, Spearman correlation), however very high speeds were not obtained (Fig. 1g, h, red; Extended Data Fig. 2b)—the maximum speed when stimulating *Vglut2⁺ChR2* PPN neurons was 19 cm s^{-1} , compared with 56 cm s^{-1} for *Vglut2⁺ChR2* CnF neurons ($P < 0.001$, Mann–Whitney *U*-test; Fig. 1i, Supplementary Video 2). Gallop and bound were also not induced upon increasing the stimulation frequency (Fig. 1g, j, bottom). In addition, the onset of the initiation of locomotion was significantly longer (0.2–1.5 s) after the stimulation of *Vglut2⁺ChR2* PPN neurons compared with *Vglut2⁺ChR2* CnF neurons (Extended Data Fig. 2c, red line; $P < 0.05$, Mann–Whitney *U*-test). Stimulation of *Vglut2⁺ChR2* PPN neurons (expression of ChR2 in Extended Data Fig. 1b) during ongoing locomotion modulated the speed ($P = 0.03$, Wilcoxon signed-rank test, causing an overall increase in speed of 18% compared with that before light onset (Extended Data Fig. 2d). However, the speed after stimulation remained within the ranges of walk and trot, confirming that selective activation of *Vglut2⁺ChR2* PPN neurons could not initiate fast, synchronous gaits.

h. Maximum speeds evoked by stimulation of the PPN (red; $N = 5$ mice, $n = 67$ trials) and the CnF (blue; $N = 9$ mice, $n = 131$ trials). Error bars indicate the 25th and 75th percentiles of the distribution. **i.** The fraction of trials at a given maximum speed (inset; *** $P < 0.001$, two-tailed Mann–Whitney *U*-test). **j.** Probability of observing different gaits upon optical stimulation of neurons in the CnF (top) or the PPN (bottom).

The frequency of stimulation did not directly translate into the observed stepping frequency. However, the relationship between stepping frequency and the velocity of locomotion (Extended Data Fig. 2e) was similar to that seen during spontaneous locomotion in wild-type mice¹, showing that locomotor activity resulting from light stimulation is similar to that exhibited naturally.

The optogenetically-induced locomotor phenotypes were linked to glutamatergic neurons in PPN or CnF. Locomotion was not induced by stimulation of the local inhibitory neurons in the PPN and the CnF¹⁴, or the cholinergic cells in the PPN, and their activation slowed or stopped ongoing locomotion (Extended Data Fig. 3a–e).

Dual and singular control of locomotion

The optogenetically induced locomotor phenotypes raise the question of whether activity in glutamatergic neurons in both the PPN and the CnF, or in either location independently, is necessary to maintain ongoing locomotion at different speeds. We therefore performed experiments that selectively dampened the activity of the identified populations using the inhibitory muscarinic designer receptor hM4Di (iDREADD), which is activated by clozapine *N*-oxide (CNO)^{19,20}. *Vglut2^{Cre}* mice were bilaterally injected with iDREADDs in both structures (CnF, $N = 8$; PPN, $N = 9$; CnF and PPN, $N = 6$; injection sites shown in Extended Data Fig. 4).

In non-viral-injected mice, no difference was seen in the instantaneous speed attained on a treadmill after treatment with either saline injections or intraperitoneal CNO (1 mg kg^{-1}) (Extended Data Fig. 5a). Test mice with viral infections that received saline attained average speeds of $26\text{--}27 \text{ cm s}^{-1}$ and maximum speeds of $47\text{--}55 \text{ cm s}^{-1}$ (Fig. 2a, b), corresponding to the slow walk/trot and fast trot ranges,

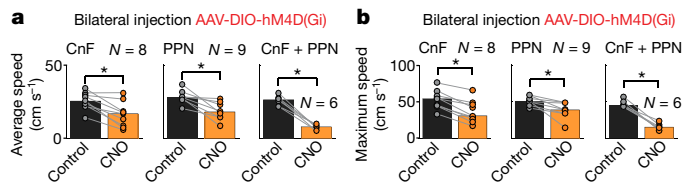


Figure 2 | The PPN and the CnF provide dual control of slower locomotion. **a, b,** Bilateral inhibition of CnF and/or PPN neurons with iDREADDs in *Vglut2^{cre}* mice. Average (**a**) and maximum (**b**) speed of mice before and after the administration of CNO (**P* < 0.05, two-tailed Wilcoxon signed-rank test).

respectively, of spontaneous locomotion in untreated adult mice¹. When *Vglut2⁺*iDREADD CnF neurons were inactivated, there was a reduction in both the average and the maximum speed (before versus after CNO treatment, average speed 27 cm s⁻¹ versus 20 cm s⁻¹, maximum speed 50 cm s⁻¹ versus 41 cm s⁻¹, Mann–Whitney *U*-test *P* < 0.05, Fig. 2a, b); similar results were obtained when *Vglut2⁺*iDREADD PPN neurons were inhibited (average speed 27 cm s⁻¹ versus 18 cm s⁻¹, maximum speed 54 cm s⁻¹ versus 43 cm s⁻¹, Mann–Whitney *U*-test *P* < 0.05, Fig. 2a, b). These effects developed over time, with the maximum effects observed after 30 min (Extended Data Fig. 5b–g). Notably, when the iDREADD virus was injected in both the PPN and the CnF bilaterally, the mice could achieve only very slow forward locomotion—typically single steps with an overall speed within the walking range (Fig. 2a, b).

These experiments suggest that glutamatergic subpopulations in both the PPN and the CnF in conjunction are necessary to maintain ongoing locomotion in the walk and trot range, and that both the PPN and the CnF can independently support slower, alternating locomotion within the walking range.

To investigate the ability of *Vglut2⁺*CnF neurons to initiate the gaits gallop and bound, we first tested the inactivation of *Vglut2⁺*iDREADD CnF neurons in a behavioural assay that allowed for fast, escape-like behaviour (Fig. 3a; Methods). Under control conditions (that is, before CNO treatment), high-speed, escape-like locomotion involving

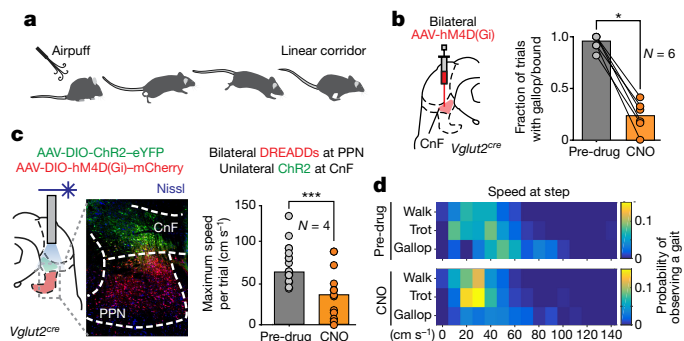


Figure 3 | Glutamatergic neurons in the CnF are required and are sufficient for fast, synchronous locomotion. **a,** To induce fast, escape-like locomotion, air puffs are applied to the back of the mouse when situated at the beginning of a linear corridor. **b,** Bilateral injection of iDREADDs in the CnF of *Vglut2^{cre}* mice (left) and the probability of evoking the gaits of gallop and/or bound during air-puff-induced escape behaviour, before and after inactivation of the CnF with CNO (*P* = 0.0312, two-tailed Wilcoxon signed-rank test, *N* = 6). **c,** Injection and expression of AAV-ChR2 in the CnF (left, green) and iDREADDs in the PPN (left, red) and fibre placement. Maximum speeds of locomotion (right) combining iDREADDs in the PPN and optogenetic activation of the CnF at 50 Hz, both before (grey; *n* = 13 repetitions, *N* = 4 mice) and after (orange; *n* = 12 repetitions, *N* = 4 mice) the administration of CNO. *P* < 0.05, two-tailed Mann–Whitney *U*-test. **d,** Probability of observing different gaits upon stimulation of neurons as described in **c**. Drawing in Fig. 3a reproduced with permission from Mattias Karlén.

gallop or bound was observed in 94% of the trials (66 out of 70, *N* = 6, Fig. 3b). After treatment with CNO, the same mice were unable to produce high-speed escape-like actions, and showed no or only isolated signs of gallop or bound in 23% of the trials (18 of 79 trials, *N* = 6, *P* < 0.05, Wilcoxon signed-rank test; Fig. 3b). We next tested if gallop and bound could be initiated upon activation of the *Vglut2⁺* CnF neurons independently of a functioning PPN, by bilateral injection of iDREADDs into *Vglut2⁺*PPN neurons and ChR2 into *Vglut2⁺*CnF neurons (Fig. 3c, *N* = 4). Light activation of *Vglut2⁺*CnF neurons induced a range of locomotor speeds, and all gaits—including gallop and bound—both before and after CNO injection, with only a reduction in the maximum speeds observed after CNO treatment (Fig. 3c, d; Supplementary Video 3). These results show that glutamatergic neurons in the CnF are necessary for producing gallop and bound, and that they can induce these gaits independently of the glutamatergic neurons in the PPN.

Neuronal firing and its relationship to speed

The complementary roles of glutamatergic neurons in the CnF and the PPN in regulating the speed of alternating locomotion may be reflected in their firing activity. We therefore recorded the activity of CnF and PPN neurons extracellularly when mice were walking or trotting on a treadmill (0–30 cm s⁻¹). Glutamatergic neurons were infected with AAV-DIO-ChR2 in either the CnF (*N* = 2) or the PPN (*N* = 2), and identified as infected by their short latency (up to 5 ms) and constant jitter responses to brief pulses of blue light (Fig. 4; Extended Data Fig. 6a). We recorded from a total of 169 *Vglut2⁺*CnF neurons and 493 *Vglut2⁺*PPN neurons; Figure 4a, b shows example neurons in the two structures. The *Vglut2⁺*ChR2 CnF neuron (Fig. 4a) showed a notable correlation between speed and firing rate. The depicted *Vglut2⁺*ChR2 PPN neurons were recruited at the beginning of the locomotor bout

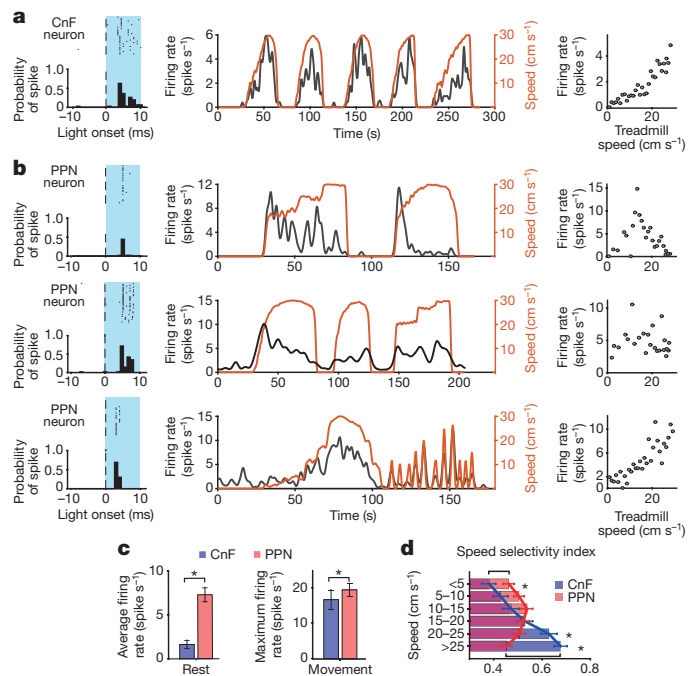


Figure 4 | Coding of speed in glutamatergic neurons in the CnF and the PPN. **a, b,** Firing of example neurons at different locomotion speeds, recorded in the CnF (**a**) and the PPN (**b**). **c,** Average (left, at rest) and maximum (right, during movement) neuronal firing rates in the CnF (*n* = 79) and the PPN (*n* = 105). *P* < 0.001, two-tailed Mann–Whitney *U*-test. **d,** Speed selectivity index. *Vglut2⁺*PPN neurons were more selective at lower speeds, whereas *Vglut2⁺*CnF neurons were more selective at higher speeds. **P* < 0.05, two-tailed Mann–Whitney *U*-test with post hoc Bonferroni correction. Data are mean ± s.e.m.

and then slowly derecruited (Fig. 4b, top), showed no modulation with speed (Fig. 4b, middle), or showed a clear modulation with the speed of locomotion (Fig. 4b, bottom).

For further quantitative analysis, we considered only the glutamatergic neurons in the PPN and the CnF for which the firing rate was modified upon changes in speed (Spearman correlation $P < 0.01$; PPN, $n = 105$, median correlation 0.63; CnF, $n = 79$, median correlation 0.63) (Extended Data Fig. 6b). Among these cells, differences were observed between the firing distributions of $Vglut2^+$ ChR2 CnF neurons and $Vglut2^+$ ChR2 PPN neurons during rest and movement (Fig. 4c, rest: average activity CnF 1.62 versus PPN 7.27; movement: maximum activity CnF 16.75 versus PPN 19.53; both $P < 0.05$, Mann–Whitney U -test).

We quantified these firing profiles by computing a speed selectivity index, which weights how much stronger the firing rate is at a specific speed compared to the activity at rest (Fig. 4d). Neurons in both the CnF and the PPN showed selectivity with respect to their baselines (Fig. 4d, $P < 0.05$, Wilcoxon signed-rank test against baseline with post hoc Bonferroni correction). Nevertheless, the selectivity was different: $Vglut2^+$ ChR2 PPN neurons were more selective at the lowest treadmill speed (below 5 cm s^{-1}) whereas $Vglut2^+$ ChR2 CnF neurons were more selective at the highest treadmill speed (above 20 cm s^{-1}) ($P < 0.05$, Mann–Whitney U -test with post hoc Bonferroni correction).

The relationship between firing rate and speed supports the suggestion that glutamatergic neurons in both the CnF and the PPN contribute towards programming the speed of alternating gait locomotion. At the lowest speeds, the PPN neurons have a greater contribution than those of the CnF, whereas the CnF neurons show the strongest contribution at higher speeds.

The PPN is involved in exploratory behaviour

The different firing behaviour of the PPN and the CnF neurons raises the possibility that they might be mobilized differently to support slow, explorative behaviour. We therefore measured explorative behaviour using the hole-board test^{21,22} (Fig. 5a), a context that encourages slow-speed locomotion for exploratory purposes. Mice were injected bilaterally with iDREADDs targeting $Vglut2^+$ neurons in either the CnF or the PPN (Fig. 5b, c). Changes in locomotion induced by $Vglut2^+$ iDREADD CnF neurons or $Vglut2^+$ iDREADD PPN neurons were measured by the average speed of locomotion, the distance travelled and the ambulation time in the same mouse after the injection of either saline or CNO. CnF-injected mice ($N = 6$) did not show any differences in these locomotor parameters (Wilcoxon signed-rank test, saline versus CNO, $P > 0.05$), whereas PPN-injected mice ($N = 6$) showed a significant reduction in the total distance travelled and the average speed (Wilcoxon signed-rank test, saline versus CNO, $P < 0.05$) (data not shown). As a measure of exploration, we measured the number and the fraction of time of head-dips. Before and after the inactivation of $Vglut2^+$ iDREADD CnF neurons, there was no difference in these parameters (Fig. 5b, $N = 6$; $P > 0.05$, Wilcoxon signed-rank test), however both were significantly reduced upon the inactivation of $Vglut2^+$ iDREADD PPN neurons, (Fig. 5c, $N = 6$; $P < 0.05$, Wilcoxon signed-rank test). These results support the suggestion that glutamatergic PPN activity may facilitate slow, explorative locomotor behaviour.

Next, we tested whether PPN activation could also increase exploration. $Vglut2^+$ neurons in the CnF or the PPN ($N = 2$ and 4, respectively; Extended Data Fig. 7) were infected with ChR2 (Fig. 5d, e) and stimulated for 10 s (40 Hz) at random times throughout the five-minute exploration period (Supplementary Video 4). There was a significant reduction in head-dipping before and after stimulation of the CnF (Fig. 5d, $P < 0.05$, Mann–Whitney U -test, $n = 40$ repetitions in $N = 2$ mice)—due to the induction of escape-like behaviour—but a significant increase in both the number and the fraction of time of head-dips during stimulation of the PPN (Fig. 5e, $P < 0.05$, Mann–Whitney U -test, $n = 53$ repetitions in $N = 4$ mice). These experiments further support the idea that activity in $Vglut2^+$ PPN neurons facilitates movements at slow speeds for the purpose of explorative behaviour.

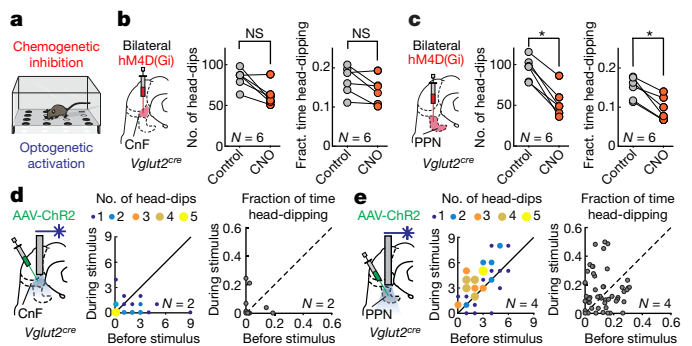


Figure 5 | Selection of exploration from the PPN. **a**, Set-up of the exploratory hole-board experiments. **b**, Bilateral inactivation of the CnF (left, $N = 6$) did not reduce either the frequency of head-dips (middle, $P > 0.05$) or the fraction of time spent head-dipping (right, $P > 0.05$). **c**, Bilateral inactivation of the PPN (left, $N = 6$) reduced both the frequency of head-dips (middle, $P = 0.031$) and the fraction of time spent head-dipping (right, $P = 0.031$). **d**, Optogenetic stimulation of the CnF (left, $N = 2$) induced a decrease in the number of head-dips (middle, $P = 0.0023$) but not in the fraction of time spent head-dipping (right, $P > 0.05$). **e**, Stimulation of the PPN (left, $N = 4$) increased both the number of head-dips (middle, $P < 0.001$) and the fraction of time spent head-dipping (right, $P = 0.0218$). All statistical tests were two-tailed Wilcoxon signed-rank tests. Drawing in Fig. 5a reproduced with permission from Mattias Karlén.

Brain-wide inputs to the CnF and the PPN

To investigate the regulation of glutamatergic excitatory neurons of the CnF and the PPN, we traced the sources of neuronal inputs into each structure using rabies-based mono-synaptically restricted retrograde trans-synaptic circuit tracing (refs 23, 24; Methods; Fig. 6). Trans-synaptically labelled neurons are visualized as red-only neurons in Fig. 6a. The overall distribution of projecting neurons to the $Vglut2^+$ CnF neurons or the $Vglut2^+$ PPN neurons was visibly different (orange dots in Fig. 6b; PPN, $N = 3$; CnF, $N = 3$). Most inputs were ipsilateral to the injection site, and inputs to $Vglut2^+$ CnF neurons were more restricted compared to those of the $Vglut2^+$ PPN neurons. The main inputs to $Vglut2^+$ PPN neurons originate in midbrain structures (Fig. 6c) and sensory-motor and raphe nuclei in the brainstem (Fig. 6d). Furthermore, $Vglut2^+$ PPN neurons also receive direct input from the output nuclei in the basal ganglia (Fig. 6e, f). Sparse inputs were found from sensory-motor and frontal cortices or the hypothalamus (Fig. 6c). Therefore, $Vglut2^+$ PPN neurons integrate sensory-motor information from many brain structures. Conversely, $Vglut2^+$ CnF neurons receive little input from basal ganglia output nuclei (Fig. 6e, f) or from cortices, but stronger projections from midbrain structures (for example the periaqueductal grey or the inferior colliculus, Fig. 6c, d) that have been assigned a role in escape responses^{25,26}.

Lastly, $Vglut2^+$ neurons in the CnF and the PPN have reciprocal projections, with dominant projections from the CnF to the PPN (Extended Data Fig. 8); these provide gateways for $Vglut2^+$ CnF neurons to modulate PPN neurons in the range of slower, alternating locomotion.

Convergent and divergent outputs

Descending projections from $Vglut2^+$ CnF neurons and $Vglut2^+$ PPN neurons were evaluated using transmitter-specific anterograde tracing (Extended Data Fig. 9a). Few neurons projected directly to the cervical and thoracic spinal cord (see also refs 27–29) (Extended Data Fig. 9c–5). $Vglut2^+$ PPN neurons have broad—predominantly ipsilateral—projections, including to motor-related nuclei in the pons as well as to modulatory nuclei (Extended Data Fig. 9b, c1–4). Most of these brainstem nuclei project to the spinal cord in mice²⁷. By contrast, the CnF has more restricted projection, and both overlapping and non-overlapping projections with the PPN in the medulla (Extended Data Fig. 9c1–4).

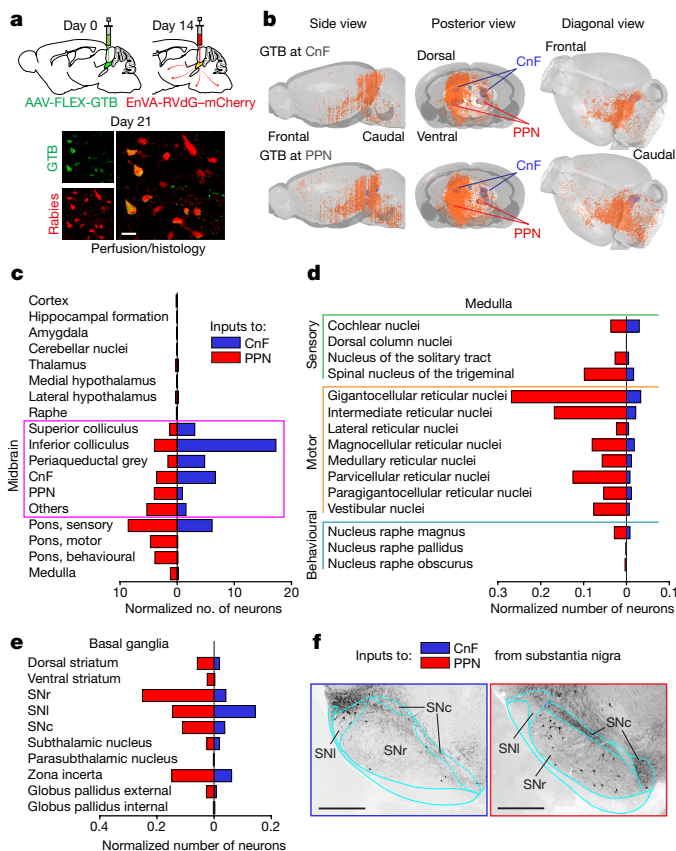


Figure 6 | Neurons in the CnF and the PPN have differential input matrices. **a**, Timeline of mono-synaptically restricted trans-synaptic retrograde tracing. Bottom, neurons infected with GTB (green, upper left), or rabies virus (red, lower left). Neurons co-infected with GTB and rabies shown in yellow. **b**, Reconstruction of projections to the CnF (top) and the PPN (bottom), as revealed by monosynaptically restricted trans-synaptic retrograde labelling ($N = 3$). **c–e**, Regional distribution (median, $N = 3$) of neurons projecting to the CnF (blue) and to the PPN (red), normalized to the number of primary infected neurons in either structure. **f**, Examples of labelled neurons (black) in the substantia nigra projecting onto glutamatergic CnF (left) or PPN (right) neurons. Scale bars: **a**, $20\ \mu\text{m}$; **f**, $500\ \mu\text{m}$. SNc, substantia nigra pars compacta; SNI, substantia nigra pars lateralis; SNr, substantia nigra pars reticulata. The mouse brain schematics in this figure have been reproduced with permission from Elsevier³⁸.

Conclusions

Our study shows that two transmitter-defined and spatially segregated populations of neurons in the mouse midbrain form command pathways that encode speeds of locomotion in complementary ways. Neuronal circuits in the PPN and the CnF both contribute to the maintenance and speed regulation of slower locomotion, whereas only the CnF is able to elicit high-speed, synchronous locomotor activity. The functional locomotor signatures are linked to the activity of the glutamatergic neurons in the CnF and the PPN. The focus on speed control and the selection of gaits provide a combined solution to understanding the functional organization of the midbrain structures involved in locomotor control. The concept of a unitary mesencephalic locomotor region in mammals is therefore refined by a more advanced model, in which the locomotor control function resides in both the PPN and the CnF.

The support of slow explorative and fast escape behaviour by glutamatergic PPN and CnF neurons, respectively, suggests that these neuronal circuits may be recruited in specific behavioural contexts. The differential input matrices into glutamatergic neurons in the CnF or the PPN also suggest the existence of dual functions in addition to the combined control of alternating gaits. The strong inputs into

Vglut2⁺CnF neurons from the periaqueductal grey (especially the dorsal part), the inferior colliculus and the hypothalamus are in accordance with previous anatomical findings¹² and suggest that CnF-mediated fast locomotion may be generated as part of an escape response independent of the PPN. As previously shown, PPN neurons receive rich projections from basal ganglia nuclei^{12,14}, but also from many midbrain and medullary sensory-motor nuclei as well as from the motor cortex. This innervation pattern is in accordance with a role of glutamatergic PPN neurons in exploratory locomotor behaviour under the motor action selection of the basal ganglia^{7,30–34}. The strong connection from the basal ganglia also suggests that dysregulation of glutamatergic neurons in the PPN may have important roles in locomotor disability related to Parkinson's disease.

The descending projections from glutamatergic CnF and PPN neurons suggest that the speed signal is funnelled through diverse brainstem nuclei, which in turn project to the locomotor networks in the spinal cord. The convergent projections of the CnF and the PPN to regions that contain excitatory reticulospinal neurons^{35,36} provide a gateway to support alternating gaits in a speed-dependent manner³⁷. This area may also be accessed from the CnF independent of the PPN, as the CnF can initiate gallop and bound without activity in the PPN. Conversely, neurons in the PPN project more broadly to nuclei in the pons and the medulla, which are mostly devoid of CnF projections, and may provide descending pathway(s) involved in slow, explorative locomotor behaviour.

Online Content Methods, along with any additional Extended Data display items and Source Data, are available in the online version of the paper; references unique to these sections appear only in the online paper.

Received 3 February; accepted 8 December 2017.

Published online 17 January 2018.

- Bellardita, C. & Kiehn, O. Phenotypic characterization of speed-associated gait changes in mice reveals modular organization of locomotor networks. *Curr. Biol.* **25**, 1426–1436 (2015).
- Grillner, S. The motor infrastructure: from ion channels to neuronal networks. *Nat. Rev. Neurosci.* **4**, 573–586 (2003).
- Kiehn, O. Decoding the organization of spinal circuits that control locomotion. *Nat. Rev. Neurosci.* **17**, 224–238 (2016).
- Grillner, S. & Jessell, T. M. Measured motion: searching for simplicity in spinal locomotor networks. *Curr. Opin. Neurobiol.* **19**, 572–586 (2009).
- Brownstone, R. M. & Wilson, J. M. Strategies for delineating spinal locomotor rhythm-generating networks and the possible role of Hb9 interneurons in rhythmicogenesis. *Brain Res. Rev.* **57**, 64–76 (2008).
- Goulding, M. Circuits controlling vertebrate locomotion: moving in a new direction. *Nat. Rev. Neurosci.* **10**, 507–518 (2009).
- Jordan, L. M., Liu, J., Hedlund, P. B., Akay, T. & Pearson, K. G. Descending command systems for the initiation of locomotion in mammals. *Brain Res. Rev.* **57**, 183–191 (2008).
- Dubuc, R. *et al.* Initiation of locomotion in lampreys. *Brain Res. Rev.* **57**, 172–182 (2008).
- Takakusaki, K., Chiba, R., Nozu, T. & Okumura, T. Brainstem control of locomotion and muscle tone with special reference to the role of the mesopontine tegmentum and medullary reticulospinal systems. *J. Neural Transm. (Vienna)* **123**, 695–729 (2016).
- Shik, M. L., Severin, F. V. & Orlovsky, G. N. Control of walking and running by means of electrical stimulation of the mesencephalon. *Electroencephalogr. Clin. Neurophysiol.* **26**, 549 (1969).
- García-Rill, E., Hyde, J., Kezunovic, N., Urbano, F. J. & Petersen, E. The physiology of the pedunculopontine nucleus: implications for deep brain stimulation. *J. Neural Transm. (Vienna)* **122**, 225–235 (2015).
- Ryczko, D. & Dubuc, R. The multifunctional mesencephalic locomotor region. *Curr. Pharm. Des.* **19**, 4448–4470 (2013).
- Martinez-Gonzalez, C., Bolam, J. P. & Mena-Segovia, J. Topographical organization of the pedunculopontine nucleus. *Front. Neuroanat.* **5**, 22 (2011).
- Roseberry, T. K. *et al.* Cell-type-specific control of brainstem locomotor circuits by basal ganglia. *Cell* **164**, 526–537 (2016).
- Wang, H. L. & Morales, M. Pedunculopontine and laterodorsal tegmental nuclei contain distinct populations of cholinergic, glutamatergic and GABAergic neurons in the rat. *Eur. J. Neurosci.* **29**, 340–358 (2009).
- Borgius, L., Restrepo, C. E., Leao, R. N., Saleh, N. & Kiehn, O. A transgenic mouse line for molecular genetic analysis of excitatory glutamatergic neurons. *Mol. Cell. Neurosci.* **45**, 245–257 (2010).
- Machado, A. S., Darmohray, D. M., Fayad, J., Marques, H. G. & Carey, M. R. A quantitative framework for whole-body coordination reveals specific deficits in freely walking ataxic mice. *eLife* **4**, e07892 (2015).

18. Lemieux, M., Josset, N., Roussel, M., Couraud, S. & Bretzner, F. Speed-dependent modulation of the locomotor behavior in adult mice reveals attractor and transitional gaits. *Front. Neurosci.* **10**, 42 (2016).
19. Roth, B. L. DREADDs for neuroscientists. *Neuron* **89**, 683–694 (2016).
20. Sternson, S. M. & Roth, B. L. Chemogenetic tools to interrogate brain functions. *Annu. Rev. Neurosci.* **37**, 387–407 (2014).
21. Kliethermes, C. L. & Crabbe, J. C. Pharmacological and genetic influences on hole-board behaviors in mice. *Pharmacol. Biochem. Behav.* **85**, 57–65 (2006).
22. File, S. E. & Wardill, A. G. Validity of head-dipping as a measure of exploration in a modified hole-board. *Psychopharmacologia* **44**, 53–59 (1975).
23. Callaway, E. M. & Luo, L. Monosynaptic circuit tracing with glycoprotein-deleted rabies viruses. *J. Neurosci.* **35**, 8979–8985 (2015).
24. Wall, N. R., Wickersham, I. R., Cetin, A., De La Parra, M. & Callaway, E. M. Monosynaptic circuit tracing *in vivo* through Cre-dependent targeting and complementation of modified rabies virus. *Proc. Natl Acad. Sci. USA* **107**, 21848–21853 (2010).
25. Brandão, M. L., Anseloni, V. Z., Pandóssio, J. E., De Araújo, J. E. & Castilho, V. M. Neurochemical mechanisms of the defensive behavior in the dorsal midbrain. *Neurosci. Biobehav. Rev.* **23**, 863–875 (1999).
26. Lovick, T. A. The periaqueductal gray-rostral medulla connection in the defence reaction: efferent pathways and descending control mechanisms. *Behav. Brain Res.* **58**, 19–25 (1993).
27. Liang, H., Paxinos, G. & Watson, C. Spinal projections from the presumptive midbrain locomotor region in the mouse. *Brain Struct. Funct.* **217**, 211–219 (2012).
28. Ryczko, D. *et al.* Forebrain dopamine neurons project down to a brainstem region controlling locomotion. *Proc. Natl Acad. Sci. USA* **110**, E3235–E3242 (2013).
29. Skinner, R. D., Kinjo, N., Ishikawa, Y., Biedermann, J. A. & Garcia-Rill, E. Locomotor projections from the pedunculopontine nucleus to the medioventral medulla. *Neuroreport* **1**, 207–210 (1990).
30. Costa, R. M. Plastic corticostriatal circuits for action learning: what's dopamine got to do with it? *Ann. N. Y. Acad. Sci.* **1104**, 172–191 (2007).
31. Grillner, S., Robertson, B. & Stephenson-Jones, M. The evolutionary origin of the vertebrate basal ganglia and its role in action selection. *J. Physiol. (Lond.)* **591**, 5425–5431 (2013).
32. Friend, D. M. & Kravitz, A. V. Working together: basal ganglia pathways in action selection. *Trends Neurosci.* **37**, 301–303 (2014).
33. Sinnamoni, H. M. Preoptic and hypothalamic neurons and the initiation of locomotion in the anesthetized rat. *Prog. Neurobiol.* **41**, 323–344 (1993).
34. Graybiel, A. M. & Grafton, S. T. The striatum: where skills and habits meet. *Cold Spring Harb. Perspect. Biol.* **7**, a021691 (2015).
35. Noga, B. R., Kriellaars, D. J., Brownstone, R. M. & Jordan, L. M. Mechanism for activation of locomotor centers in the spinal cord by stimulation of the mesencephalic locomotor region. *J. Neurophysiol.* **90**, 1464–1478 (2003).
36. Drew, T., Dubuc, R. & Rossignol, S. Discharge patterns of reticulospinal and other reticular neurons in chronic, unrestrained cats walking on a treadmill. *J. Neurophysiol.* **55**, 375–401 (1986).
37. Capelli, P., Pivetta, C., Esposito, M. S. & Arber, S. Locomotor speed control circuits in the caudal brainstem. *Nature* **551**, 373–377 (2017).
38. Franklin, K. B. J. & Paxinos, G. *The Mouse Brain in Stereotaxic Coordinates* 4th edn (Academic, 2013).

Supplementary Information is available in the online version of the paper.

Acknowledgements This research was supported by European Research Council grant ERC-693038 (O.K.), NINDS NS 090919 (O.K.), The Swedish Medical Research Council (O.K., G.F.), StratNeuro (O.K.) and Novo Nordisk Foundation Laureate Research grant NNF 150C0014186 (O.K.). We thank P. Löw for assistance with viral work and K. Deisseroth for providing viral Chr2 vectors.

Author Contributions O.K. initiated the project. V.Cag., R.L., H.G.-E. and O.K. designed the experiments with contributions from all authors. V.Cag. and R.L. performed optogenetic experiments, *in vivo* recordings and analysis. C.B. and H.G.-E. contributed to locomotor gait analysis, and J.B. to the initial optogenetic experiments. H.G.-E. and D.M. were responsible for chemogenetic inactivation experiments together with R.L. and V.Cag., and all analysed the data together with O.K. H.G.-E. and R.L. performed anatomical analysis with V.Cag. V.Cal. carried out *in situ* hybridizations. V.Cag. and O.K. wrote the paper with contributions from all authors. O.K. supervised all aspects of the work.

Author Information Reprints and permissions information is available at www.nature.com/reprints. The authors declare no competing financial interests. Readers are welcome to comment on the online version of the paper. Publisher's note: Springer Nature remains neutral with regard to jurisdictional claims in published maps and institutional affiliations. Correspondence and requests for materials should be addressed to O.K. (Ole.Kiehn@ki.se), V.Cag (caggiano@gmail.com) or R.L. (Roberto.Leiras@sund.ku.dk).

METHODS

Data reporting. The experiments were not randomized. For the hole-board experiments, the investigators were blinded to treatment allocation and outcome assessment. For all other experiments, the investigators were not blinded to allocation during experiments and outcome assessment. No statistical methods were used to predetermine sample size.

Mice. All experiments were approved by the local ethical committee (Stockholm Norra Djuretiska nämnden). For most experiments, adult *Vglut2^{cre}* transgenic mice¹⁶ were used (3–5 months old, of both sexes). In some experiments, adult *Vgat^{cre}* and *Chat^{cre}* (ChAT-IRES-Cre knock-in, Jackson Laboratory) transgenic mice were used (8–14 weeks old, of both sexes). *Chat^{cre}* mice were crossed with Rosa26-CAG-LSL-ChR2-eYFP-WPRE mice (Jackson Laboratory). Mice were genotyped before the experiments.

In vivo optogenetic experiments. For viral transfection of *Vglut2*-expressing neurons, *Vglut2^{cre}* mice aged 3–5 months were anaesthetized with isoflurane. For activation experiments, 100–300 nl of an AAVdj-EF1a-DIO-hChR2-p2A-mCherry-WPRE virus was pressure-injected using a glass micropipette into the CnF (anteroposterior angle 15°, from bregma: anteroposterior –5.7 mm, mediolateral 1.2 mm, depth 2.9 mm) or the PPN (anteroposterior angle 20°, from bregma: anteroposterior –5.9 mm, mediolateral 1.2 mm, depth 4.2 mm). In the same surgery, an optical fibre (200 µm core, numerical aperture 0.22, Thorlabs) held in a 1.25 mm ferrule was implanted (500 µm above the injection site) for stimulation of the transfected cells. To reduce firing in *Vglut2*-expressing neurons, 100–200 nl of an AAV-hSyn-DIO-hM4D(Gi)-mCherry virus (UNC vector core) was bilaterally injected in either the CnF or the PPN, or in both structures.

When accessing the PPN, great care was taken not to damage the CnF by adjusting the angle to 20°. By measuring the response evoked from stimulation of the CnF in mice ($N=2$) expressing ChR2 in both the CnF and the PPN, we confirmed that acutely lowering the optical fibre to stimulate first the CnF and then the PPN did not damage the CnF. Thus, the same activation of both the CnF and the PPN was obtained both when lowering and retracting the probe, demonstrating that damage to the CnF did not account for the findings in the PPN.

Some mice were injected bilaterally with AAV-hSyn-DIO-hM4D(Gi)-mCherry virus in the PPN, and unilaterally with AAVdj-EF1a-DIO-hChR2-p2A-eYFP-WPRE and implanted for optical stimulation of the CnF. For the first week after surgery, all mice were treated daily with analgesics and monitored for any sign of discomfort.

Optogenetic stimulation. A 473 nm laser (Optoduet, Ikecool Corporation) was connected to the ferrule that was chronically implanted on the mice through a ceramic mating sleeve. For light-activation of ChR2-transfected neurons, we used trains of light pulses (Master-8 pulse generator, AMPI or custom-made MATLAB (Mathworks Inc.) scripts) with variable pulse durations and frequencies. When the frequency was changed, the pulse duration was also changed to obtain the same intensity of stimulation with constant laser power. The intensity of the laser was between 5 mW and 30 mW.

Drugs. Clozapine *N*-oxide (CNO, Sigma-Aldrich) was dissolved in physiological saline to obtain a final dose of 1 mg kg⁻¹, before intraperitoneal injection.

Behavioural test in a corridor. Locomotor behaviour was recorded with the TSE MotoRater system with the mice running spontaneously on a 1.2-m long runway, as previously described^{13,39}. Videos were acquired using a high-speed camera at 300 frames per second, and analysed offline.

For the induction of fast, escape-like locomotion (gallop and bound), we used standardized air puffs (50 psi, 500 ms long) applied to the back of the mouse when it was situated at the beginning of the corridor. The test was repeated ten times with several minutes of rest between trials, both before and after intraperitoneal injection of CNO.

Behavioural test on a treadmill. Locomotion was analysed using a motorized transparent treadmill with adjustable speed range (Exer Gait XL, Columbus Instruments). The mice were conditioned to locomote on the treadmill set at constant speed, in bouts of 20 s separated by 1–2 min inter-trial periods. Ventral plane videography was recorded at 100 frames per second. Each mouse was tested at three different speeds: 0–4 cm s⁻¹, 4–20 cm s⁻¹, and >20 cm s⁻¹ before and after intraperitoneal injection of CNO. The instantaneous speed of the mice was measured throughout the experiments using custom-made MATLAB scripts with foot placement monitored from below.

Hole-board behavioural test. Exploratory behaviour was analysed using a modified version of the hole-board apparatus, consisting of test boxes made of transparent Plexiglas (45 cm × 45 cm × 41 cm) and a hole-board frame with 16 holes in a grid-pattern (2 cm diameter, 9 cm apart), placed 4 cm above the floor of the testing box. The apparatus was located in a testing room with dimmed illumination (40 lux). Odour-impregnated bedding from cages of the same gender, which is a strong exploratory motivator, was placed below the hole-board frame. To reduce habituation due to multiple trials, new social odour sources were placed

under the hole-board platform for every new trial. During the experiments, the experimenters knew whether they had injected saline or CNO, but were blind to whether the mouse had the virus injected or not; the experimenter also did not know the site of injection (that is, either CnF or PPN).

The same hole-board set-up was used to induce exploration with the stimulation of channelrhodopsin-expressing *Vglut2⁺* neurons. Mice were first tested with the MotoRater and light-activated responders were pre-selected for exploration tests. On the test day, they were placed in the open field and stimulus parameters were adjusted for each mouse in order to produce a locomotor response (typically 30–40 Hz, pulse duration 10 ms). The mice were then stimulated with trains of stimuli lasting 10 s, delivered at random intervals every 20–40 s over the five-minute test period.

Monosynaptically restricted trans-synaptic labelling. We used a glycoprotein (G)-deleted rabies virus^{23,24} pseudotyped with the envelope glycoprotein EnvA to enable the selective infection of glutamatergic cells via the TVA receptor. The TVA receptor was delivered together with the rabies glycoprotein conditionally to glutamatergic cells, by injecting 200–300 nl AAVdj-EF1a-FLEX-GTB virus (helper virus, Salk Institute, visualized in green in Fig. 6a) into either the CnF or the PPN in *Vglut2^{cre}* mice. Two weeks after the helper virus injection, 200–300 nl of an EnvA G-deleted rabies-mCherry conjugate (Salk Institute) was injected at the same location. Finally, one week after the injection of the rabies virus, mice were transcardially perfused and the tissue analysed (see ‘Sectioning, histology and imaging’).

Anterograde labelling. For anterograde labelling, 50–100 nl of cell-filling AAVdj-EF1a-DIO-hChR2-p2A-mCherry-WPRE and AAVdj-EF1a-DIO-hChR2-p2A-eYFP were injected into the CnF and the PPN, respectively. The mice were euthanized six weeks after the injection.

Sectioning, histology, and imaging. Adult mice were anaesthetized with pentobarbital and perfused with 4% (w/v) paraformaldehyde in PBS. Brains and spinal cords were removed and post-fixed for 3 h in 4% paraformaldehyde. After fixation, tissues were rinsed in PBS, cryoprotected in 25% (w/v) sucrose in PBS overnight and frozen in Neg-50 embedding medium. Coronal sections (30–40 µm thick) were cut on a cryostat.

Sections were permeabilized with PBS and 0.5% (w/v) Triton X-100 (PBST) and blocked in PBST supplemented with 5% (v/v) normal donkey serum (Jackson ImmunoResearch), before incubation for 24–48 h at 4 °C with one or several of the following primary antibodies diluted in PBST supplemented with 1% normal donkey serum: chicken anti-GFP (1:1,000, Abcam, ab13970), rabbit anti-mCherry (1:1,000, Clontech 632496), goat anti-ChAT (1:100, Millipore AB144P), rabbit anti-Cre (1:8,000, a gift from G. Shutz—see ref. 16). Secondary antibodies (F(ab')₂ fragments) were obtained from Jackson ImmunoResearch or Invitrogen, used at 1:500 and incubated for 3 h at room temperature in PBST 1% normal donkey serum. A fluorescent Nissl stain (NeuroTrace Blue 435/455, 1:200, Life Technologies) was added during the primary antibody incubation. No antibody was required to detect the rabies-mCherry labelling. Slides were rinsed, mounted in Prolong Diamond Antifade mounting medium (Life Technologies) and scanned on a confocal laser scanning microscope (LSM510 or LMS700, Zeiss Microsystems) using 10×, 20× and 40× objectives.

Fluorescent *in situ* hybridization combined with immunofluorescence labelling was performed as previously described¹⁶ using a *Vglut2* probe spanning the base pairs 540–983 (produced by L. Borgius).

Assessment of fibre placement and viral expression pattern. The assessment of the position of the optical fibre tip was based on the visible tract in the tissue. The extent of virus expression in *Vglut2^{cre}* or *Vgat^{cre}* mice was evaluated by outlining the area of expression on sections from individual mice redrawn from a mouse brain atlas, and then superimposing all mice at 30% transparency to highlight the average expression in each group (see ref. 40). Mice with no successful bilateral injections in the DREADD experiments were excluded from the analysis.

Trans-synaptic labelling experiments. For trans-synaptic labelling experiments, all sections were serially collected spanning the whole brain, from the C1 vertebral level to the olfactory bulbs. Every third section was scanned for analysis. Each slice was captured with at least two channels: one for the Nissl staining, and the other for the mCherry that enables the detection of rabies-infected neurons. In addition, a third channel was used to detect the GTB in primary-infected neurons at the site of injection. The analysis consisted of two parts. First, anatomical landmarks were identified based on the Nissl staining and matched (affine transformation followed by cubic B-spline transformation) to the coordinate framework (CCF v3) of the Allen Mouse Brain Atlas at 25-µm resolution with custom-made MATLAB scripts. Second, single neurons were automatically detected based on pixel values above the first of eight thresholds computed using Otsu's method. Then, the sections were manually checked to remove fluorescent counts that were inaccurately detected as neurons or to add neurons that were not detected automatically. Projection to the standardized Allen Mouse Brain Atlas was performed via the B-spline maps

computed in the first step. A contrast enhancement and a noise reduction filter were applied using ImageJ to images for publication.

Gait data analysis. Videos were analysed using scripts written in MATLAB. The speed of the mice was detected by colour segmentation with respect to the background and compensated for the movement of the camera in the corridor using the Lucas–Kanade method. The initiation of locomotion was defined as mouse displacement with speeds greater than 3 cm s^{-1} . Gait analysis was performed with the same methods as described previously^{1,39}. A step cycle was defined as a complete cycle of leg movement from the beginning of the stance phase (foot touchdown) to the end of the swing phase (foot touchdown again). The step frequency was defined as the inverse of the step-cycle duration. All steps were divided into four main gait on the basis of footprint analysis. The classification of steps involved visual inspection followed by quantitative evaluation of limb coordination. For quantification, we identified the beginning of the stance phase (touchdown of the foot with the ground) and the beginning of the swing phase (lift-off of the foot from the ground) for all limbs in each step. Walk is defined as a pattern of limb movement in which three or four feet are on the ground simultaneously (speed $<25\text{--}30 \text{ cm s}^{-1}$) (ref. 1). Trot is characterized by a pattern of movement in which diagonal pairs of limbs (for example, left forelimb and right hindlimb) move forward simultaneously and homologous pairs of limbs (for example, hindlimbs) are in alternation (speed $30\text{--}70 \text{ cm s}^{-1}$) (ref. 1). Bound is a pattern of movement in which the mouse moves the forelimbs and hindlimbs in synchrony throughout the movement, but with the fore- and hindlimb moving out of phase (speed $80\text{--}150 \text{ cm s}^{-1}$) (ref. 1). Gallop is characterized by synchronized hindlimb movement and out-of-phase forelimb movement (speed $60\text{--}120 \text{ cm s}^{-1}$) (ref. 1).

Neuronal recordings and analysis. Linear arrays (NeuroNexus multi-site electrode, A1-X16-5 mm-100-413) were inserted into the CnF or the PPN through a microscope. Mice were placed on a custom-built treadmill, the speed of which could be continuously changed. Movement of the treadmill, laser stimulation and array data were stored at 25 kHz on a TDT logger and analysed offline. The maximum speed of the treadmill that mice could reliably follow in a head-fixed experimental set-up was 30 cm s^{-1} . Spike sorting was performed offline by adjusting the energy level in a superparamagnetic clustering algorithm (wave_clus⁴¹, https://github.com/csn-le/wave_clus). Spike trains were aligned either to the speed of the treadmill or to the onset of the optical stimulation. Neurons infected with ChR2 were detected by their fast and reproducible response to 20 ms pulses of blue light. The neuronal activity was quantified in a window from 10 ms before light onset to 5 ms after light onset. Neurons that showed a significant increase in the instantaneous frequency of firing in the ‘after-light-onset-period’ compared to the ‘before-light-onset-period’ ($P < 0.05$, Wilcoxon signed-rank test) and had a short-latency response were considered Vglut2⁺ChR2 CnF or Vglut2⁺ChR2

PPN neurons. We calculated the instantaneous frequency of firing and speed of locomotion in 500 ms bins and quantified the relationship between the firing rate and the speed of the treadmill by averaging the firing rate every 1 cm s^{-1} . A neuron was included as speed-related when it showed a significant correlation between the firing rate and the speed of the treadmill ($P < 0.01$, Spearman correlation). A speed selectivity index was calculated as the absolute value of the average binned neuronal activity in specific speed ranges (for example, up to 5 cm s^{-1} , from 5 to 10 cm s^{-1} , etc.) minus the average neuronal activity at rest, and then divided by their sum. This index weights how much the firing rate at a specific speed is stronger than the activity at rest. It is close to 1 when the firing rate at that given speed is markedly different to the baseline.

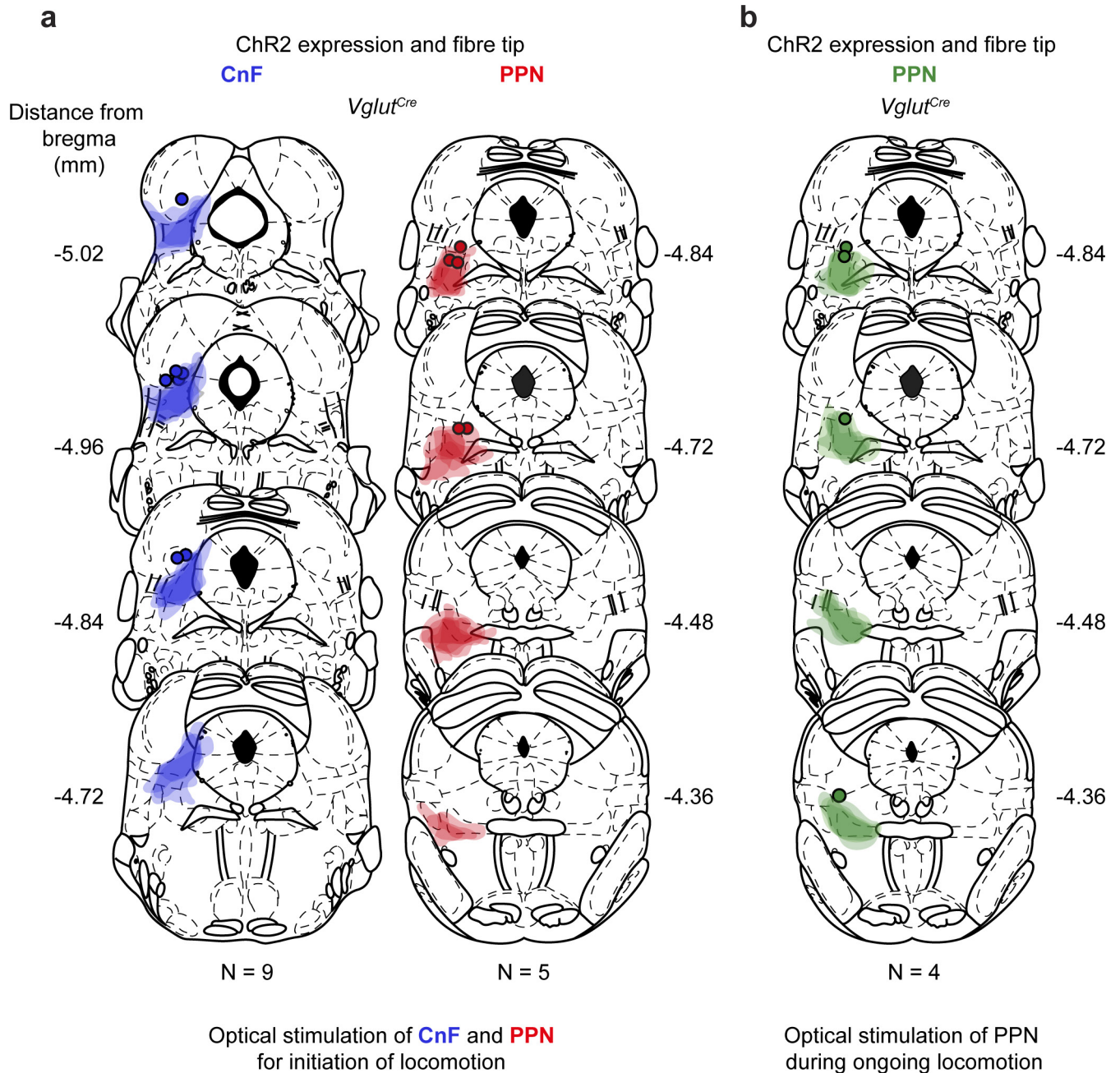
Tracking in hole-board. Head-dipping behaviour was recorded using a camera (30 frames per second) placed above the test box. Average speed, distance moved and duration of the head dips were measured using Ethovision software (Noldus Information Technology Inc.). The total number of head dips (hole visits) for each single hole was corrected by visual inspection of an experimenter blind to group and treatment. For optogenetically induced exploration, data were collected in 10 s stimulus periods. Only trials in which mice were exploring for less than 25% of the time before light stimulation were included in the analysis, to avoid behavioural adaptation.

Data availability. The datasets generated and/or analysed during the current study are available from the corresponding author upon reasonable request.

Code availability. Code used for analysis is available from the corresponding author upon reasonable request.

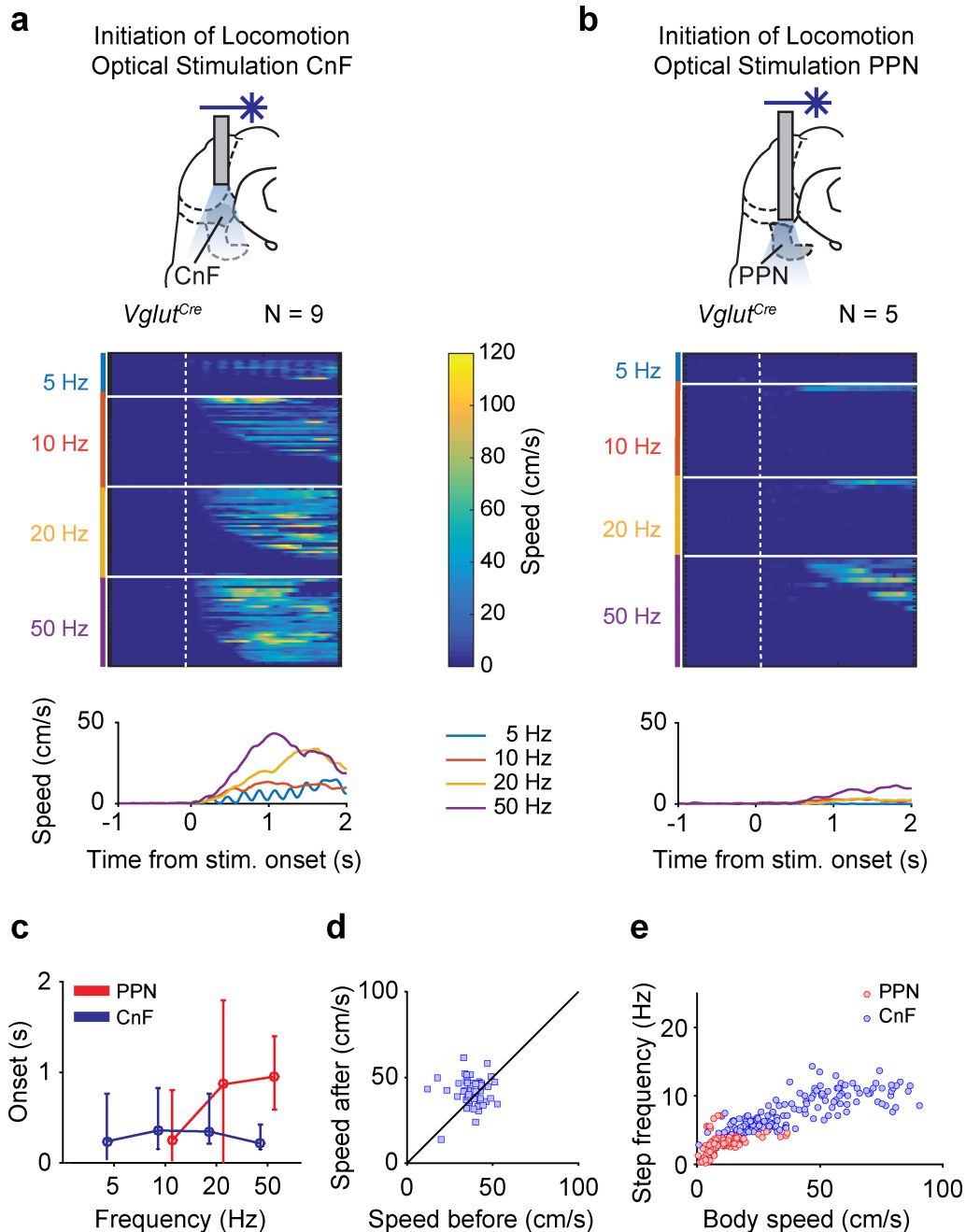
Statistics. Throughout the paper, the level of significance is indicated as * for $P < 0.05$, ** for $P < 0.01$ and *** for $P < 0.005$. All statistical tests used were two-tailed. Exact P values less than 0.001 were reported as $P < 0.001$. Non-parametric Kruskal–Wallis tests were used for non-matched data, and Friedman tests were used for repeated measurements. Correction for multiple comparisons was performed using the Bonferroni method. Custom scripts in MATLAB or R were used for the generation of graphs and statistical measurements. Wherever reported, data are medians and error bars indicate the 25th and 75th percentiles of the distribution, unless specified otherwise.

39. Bouvier, J. *et al.* Descending command neurons in the brainstem that halt locomotion. *Cell* **163**, 1191–1203 (2015).
40. Tovote, P. *et al.* Midbrain circuits for defensive behaviour. *Nature* **534**, 206–212 (2016).
41. Quiroga, R. Q., Nadasdy, Z. & Ben-Shaul, Y. Unsupervised spike detection and sorting with wavelets and superparamagnetic clustering. *Neural Comput.* **16**, 1661–1687 (2004).



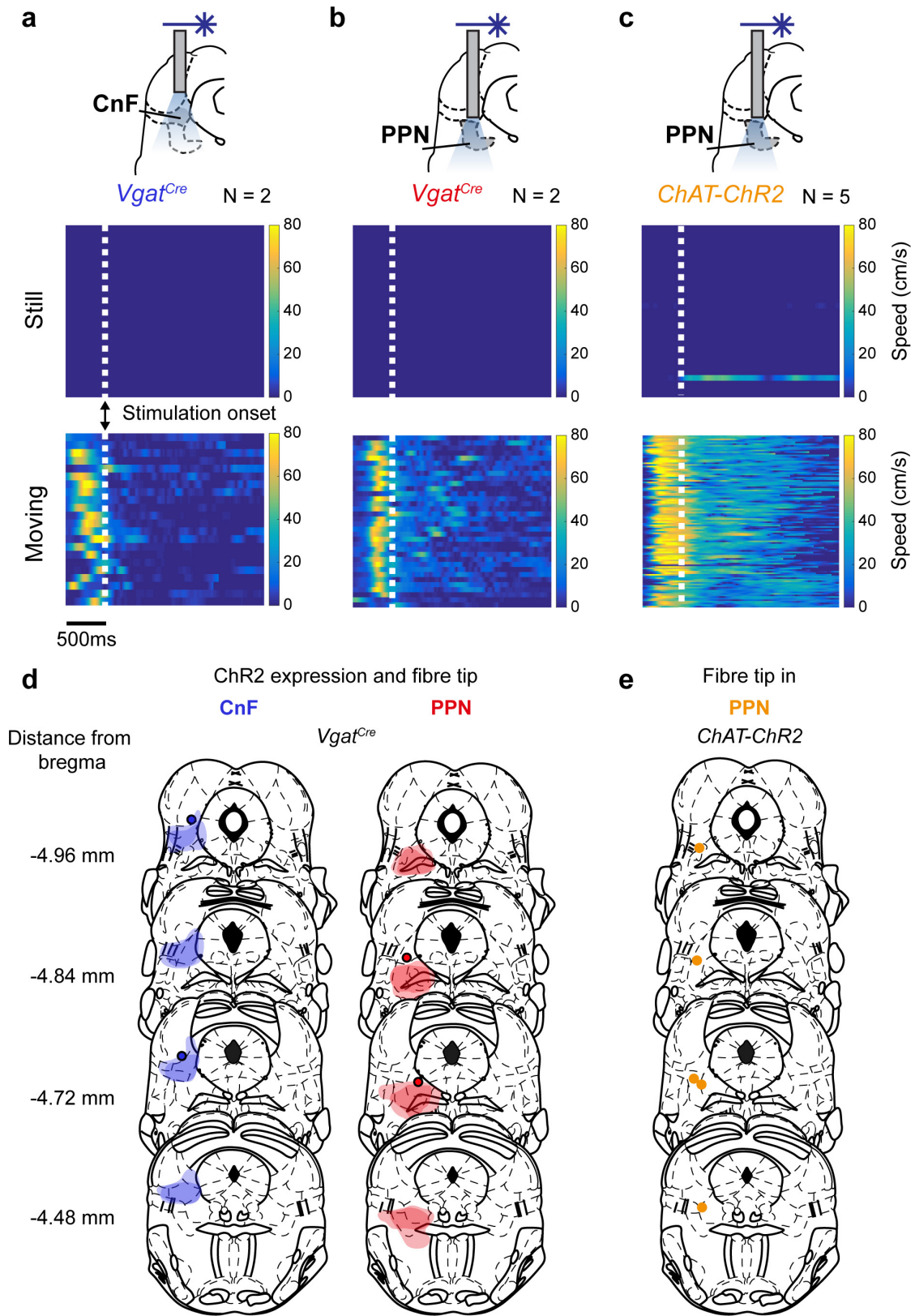
Extended Data Figure 1 | ChR2 expression in the CnF and the PPN.
This figure summarizes the behavioural data in Fig. 1 and Extended Data Fig. 2a, b. **a**, Expression of ChR2 and fibre-tip positions in the CnF (left) and the PPN (right) for the data in Fig. 1 and Extended Data Fig. 2a–c, e. Coronal brain sections with viral expression from injected *Vglut2^{Cre}* mice were superimposed on sections redrawn from a mouse brain atlas³⁸.

The darker contour colours indicate the centre of expression, whereas the lighter colours indicate the border of the most extended expression. The round dots show the tip of the fibre. **b**, Expression of ChR2 and fibre-tip positions for the PPN data in Extended Data Fig. 2d. The mouse brain schematics in this figure have been reproduced with permission from Elsevier³⁸.



Extended Data Figure 2 | Control of locomotion speed from glutamatergic neurons in the CnF and the PPN. **a, b**, Speed profiles of mice after the stimulation of *Vglut2⁺ChR2* CnF (**a**) and *Vglut2⁺ChR2* PPN (**b**) neurons. Top panels show the location of optical stimulation in the CnF (**a**) and the PPN (**b**). Middle panels show colour plots of individual trials after the stimulation of *Vglut2⁺ChR2* CnF (**a**) and *Vglut2⁺ChR2* PPN (**b**) neurons (Fig. 1). The x axis represents time and the y axis represents trials at different stimulation frequencies. Data are aligned to the onset of stimulation (stim.). The colour gradient illustrates speed, with dark blue representing no movement and colours towards yellow representing the increase in speed (up to 120 cm s^{-1})

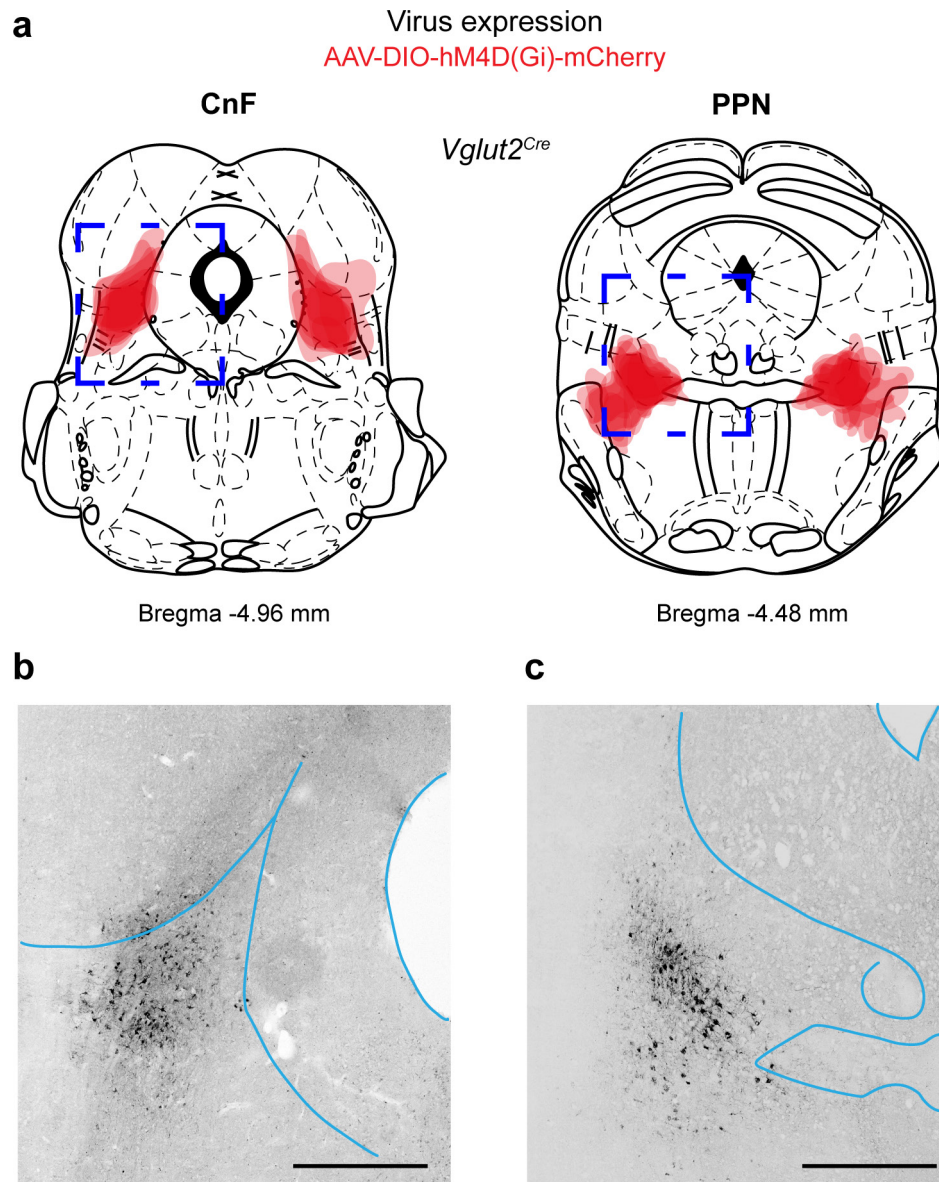
of the mouse in the linear corridor. Bottom panels show speed profiles obtained as an average of the movements at each stimulation frequency. **c**, Latencies to onset of locomotion from the stimulation of *Vglut2⁺ChR2* PPN (red) and *Vglut2⁺ChR2* CnF (blue) neurons as a function of the stimulation frequency. Error bars indicate the 25th and 75th percentiles of the distribution. **d**, Post-stimulus locomotor speed plotted against pre-stimulus locomotor speed in *Vglut2^{Cre}* mice that had been injected in the PPN with AAV-DIO-ChR2-mCherry ($n = 50$ trials from $N = 4$ mice). **e**, Step frequency plotted against speed of locomotion for the stimulation of *Vglut2⁺ChR2* PPN neurons (red, $n = 84$ trials from $N = 5$ mice) or *Vglut2⁺ChR2* CnF neurons (blue, $n = 173$ trials from $N = 9$ mice).



Extended Data Figure 3 | See next page for caption.

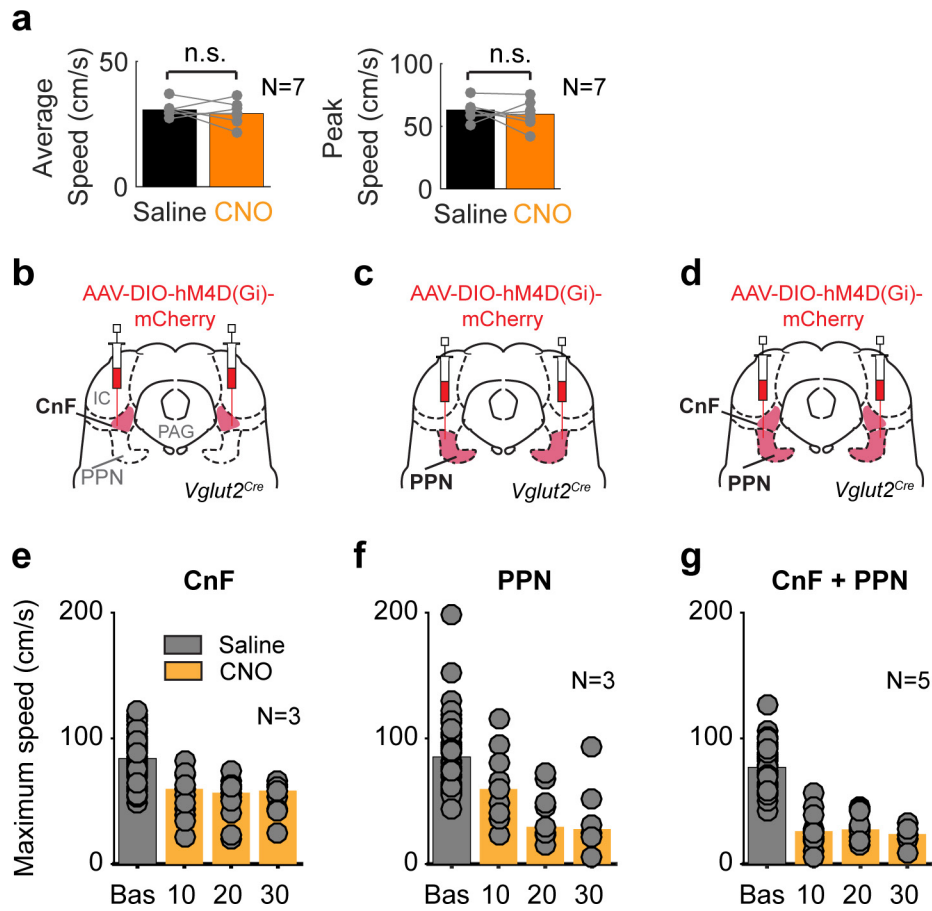
Extended Data Figure 3 | Activation of inhibitory neurons in the CnF or the PPN, and cholinergic neurons in the PPN, does not initiate locomotion but may modulate ongoing locomotion. **a–c**, Top panels show the implantation of the optical fibre to stimulate inhibitory cells in the CnF (**a**) and the PPN (**b**), and the cholinergic cells in the PPN (**c**). AAV-DIO-ChR2 virus was injected in *Vgat^{cre}* mice to target inhibitory cells, whereas cholinergic neurons expressed ChR2 transgenically by crossing *Chat^{cre}* with *RC26-ChR2^{flx/flx}* mice. Experiments were performed 3–4 weeks after injection of the virus, with mice locomoting spontaneously in a linear corridor. Middle and bottom panels show colour plots in which the *x* axis represents time and the *y* axis represents different trials, when the mice were not locomoting (middle panels, ‘still’) or when they were locomoting (bottom panels, ‘moving’) before the stimulation. Data are aligned to the onset of stimulation (dotted lines). The colour gradient illustrates speed, with dark blue representing no movement and colours

towards yellow representing an increase in speed (up to 60–80 cm s⁻¹) of the mouse in the linear corridor. Speed before versus after stimulation: CnF-*Vgat* inhibitory neurons: from still, $P > 0.05$, Wilcoxon signed-rank test (two sided) ($n = 18$, $N = 2$); when moving, from 27.9 cm s⁻¹ to 4.2 cm s⁻¹ $P < 0.05$, Wilcoxon signed-rank test ($n = 22$, $N = 2$). PPN-*Vgat* inhibitory neurons: from still, $P > 0.05$ ($n = 5$, $N = 2$); when moving from 27.6 cm s⁻¹ to 8.6 cm s⁻¹, $P < 0.05$ Wilcoxon signed-rank test (two-sided) ($n = 34$, $N = 2$). Stimulation of long-projecting cholinergic cells in the PPN: from still, $P > 0.05$, Wilcoxon signed-rank test ($n = 102$, $N = 5$); when moving: before 47.3 cm s⁻¹, after 22.9 cm s⁻¹, $P < 0.05$, Wilcoxon signed-rank test (two-sided) ($n = 88$, $N = 5$). *n*, number of trials; *N*, number of mice. **d**, Diagram of viral expression and fibre-tip positions in *Vgat^{cre}* mice in the CnF (left) and the PPN (right). **e**, Diagram of fibre-tip positions in *Chat^{cre}* mice. The mouse brain schematics in this figure have been reproduced with permission from Elsevier³⁸.



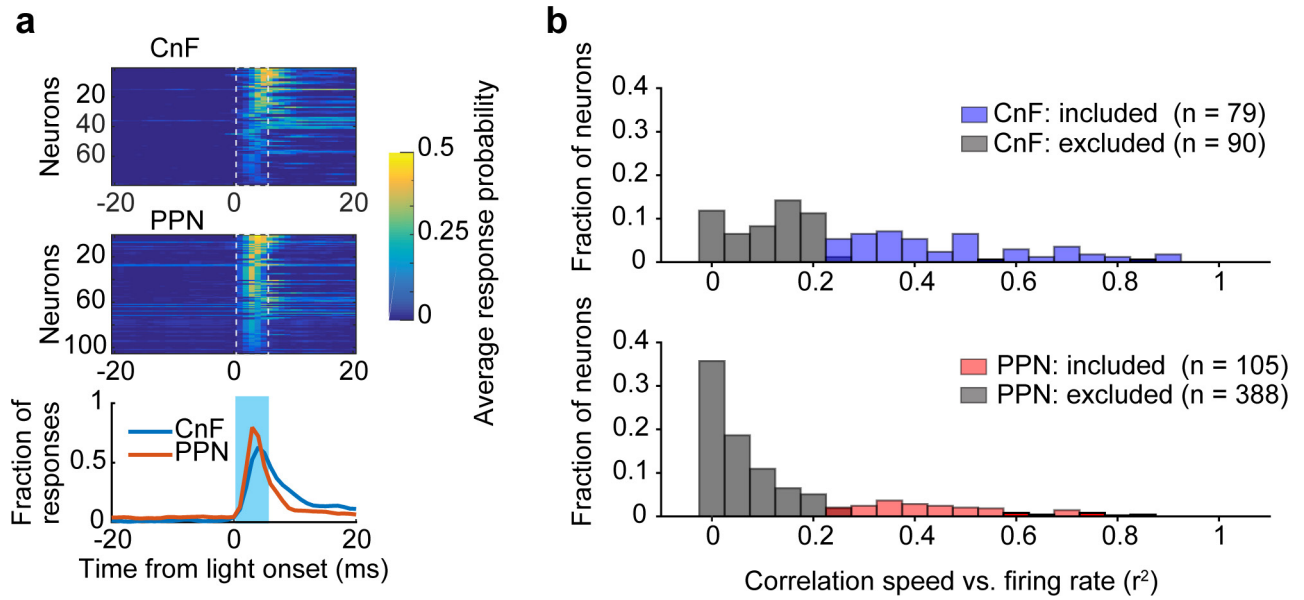
Extended Data Figure 4 | Summary diagram of iDREADD injection sites in the CnF and the PPN. **a**, Expression of iDREADD in $Vglut2^{+}$ neurons of the CnF (left, $N=8$) or the PPN (right, $N=9$) in mice used in Fig. 2. **b, c**, Coronal sections showing the expression pattern of iDREADD

in $Vglut2^{+}$ CnF (**b**) and $Vglut2^{+}$ PPN (**c**) neurons. Scale bars, $500\mu\text{m}$. The mouse brain schematics in this figure have been reproduced with permission from Elsevier³⁸.



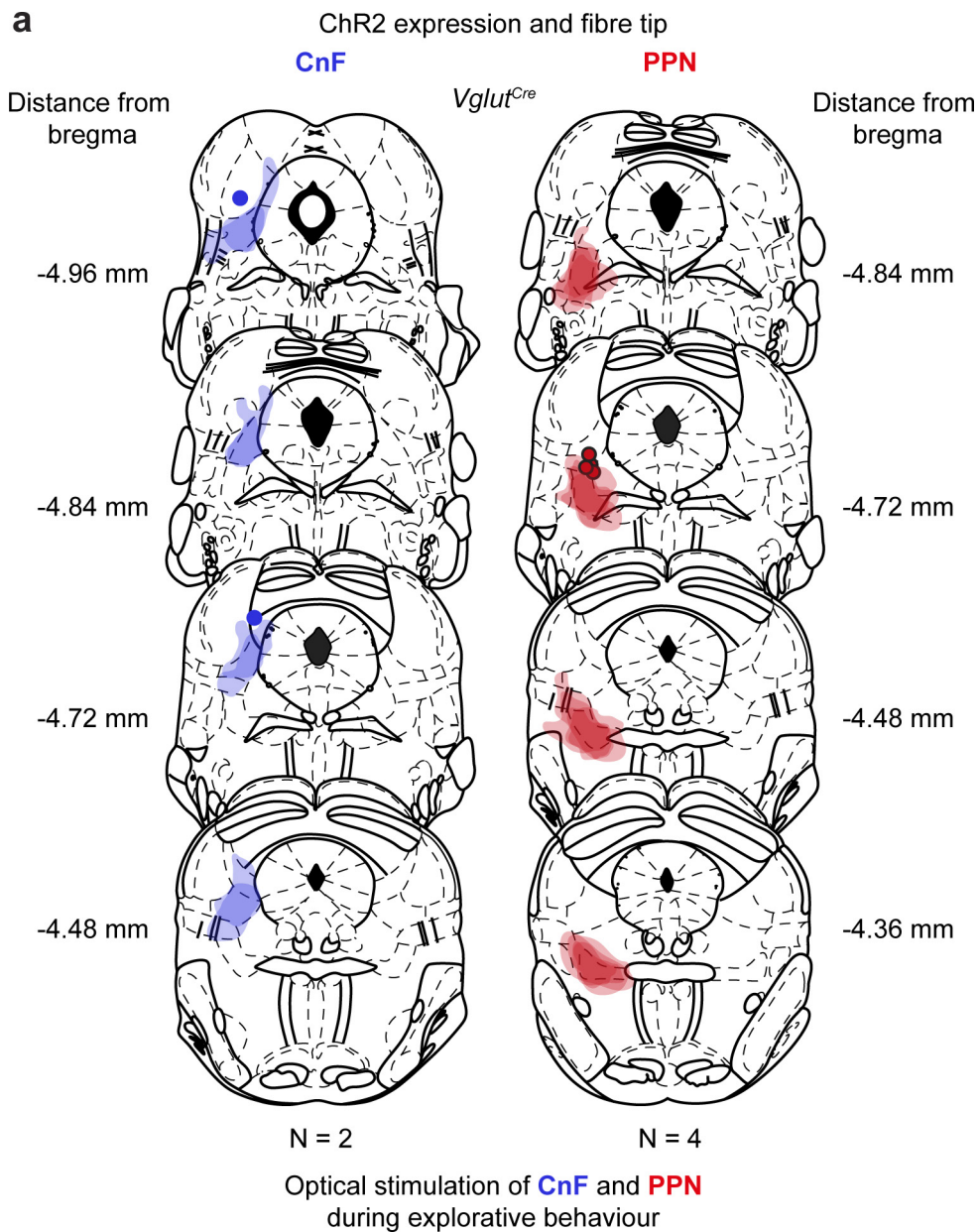
Extended Data Figure 5 | Control for CNO injection and time course of the silencing effect of glutamatergic neurons in the CnF and the PPN. **a**, Average (left) and maximum (right) speeds attained by wild-type mice during treadmill experiments after the intraperitoneal injection of saline (black) and CNO (orange, 1 mg kg^{-1}) ($N=7$). There was no significant difference in these speed parameters between the saline and CNO experiments (Wilcoxon signed-rank, two-sided, $P > 0.45$). **b–d**, Sites of

AAV-DIO-hM4D(Gi)-mCherry injection in *Vglut2^{Cre}* mice in the CnF (**b**), the PPN (**c**) or the CnF and PPN (**d**). CNO was injected intraperitoneally and locomotor performance was tested on a treadmill. **e–g**, Graphs show the development of the inhibition of glutamatergic cells in the CnF (**e**, $N=3$), the PPN (**f**, $N=3$) or the CnF and PPN (**g**, $N=5$) on maximal locomotor speed over time. Grey bars, baseline. Orange bars, time (in min) after CNO administration. Points show individual trials.



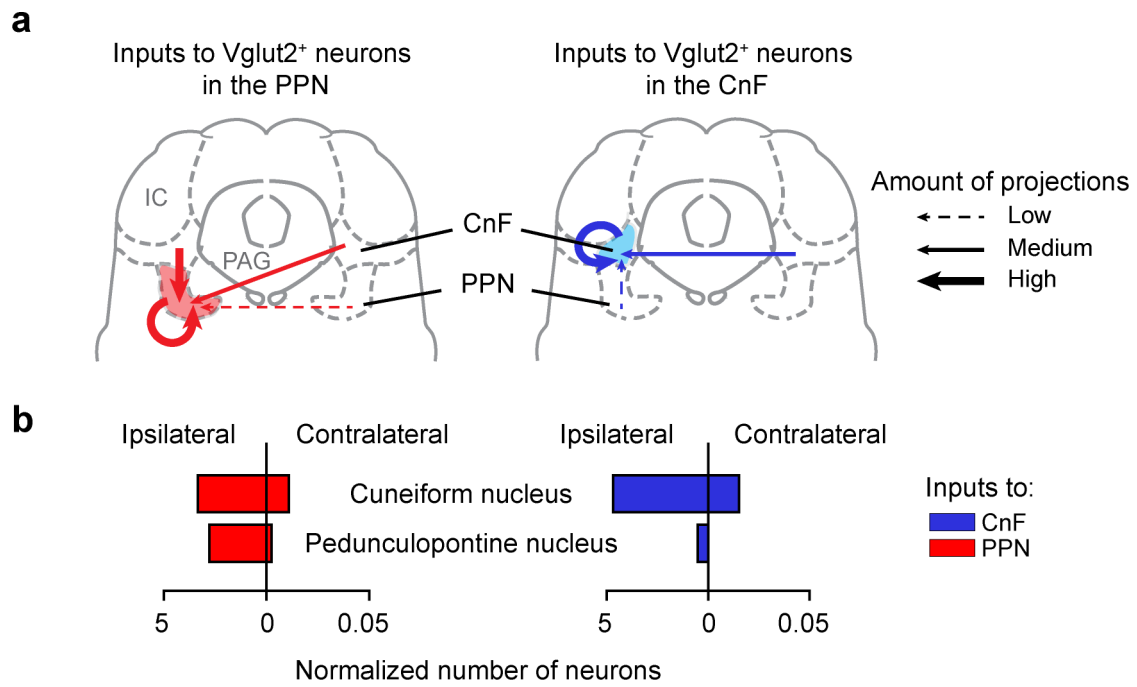
Extended Data Figure 6 | Latencies of the light activation of PPN and CnF neurons, and fractions of Vglut2⁺ChR2 neurons of the CnF and PPN with speed-related activity. **a**, Latencies of light activation of all cells included in the analysis. **b**, Distribution of Vglut2⁺ChR2 CnF neurons (blue bars, $n = 79$ out of 169) and Vglut2⁺ChR2 PPN neurons (red bars,

$n = 105$ out of 493) showing the correlation of firing activity with the locomotor speed of the mouse. In both panels, grey bars indicate neurons that show no significant correlation with the speed (Spearman correlation test, $P > 0.05$).



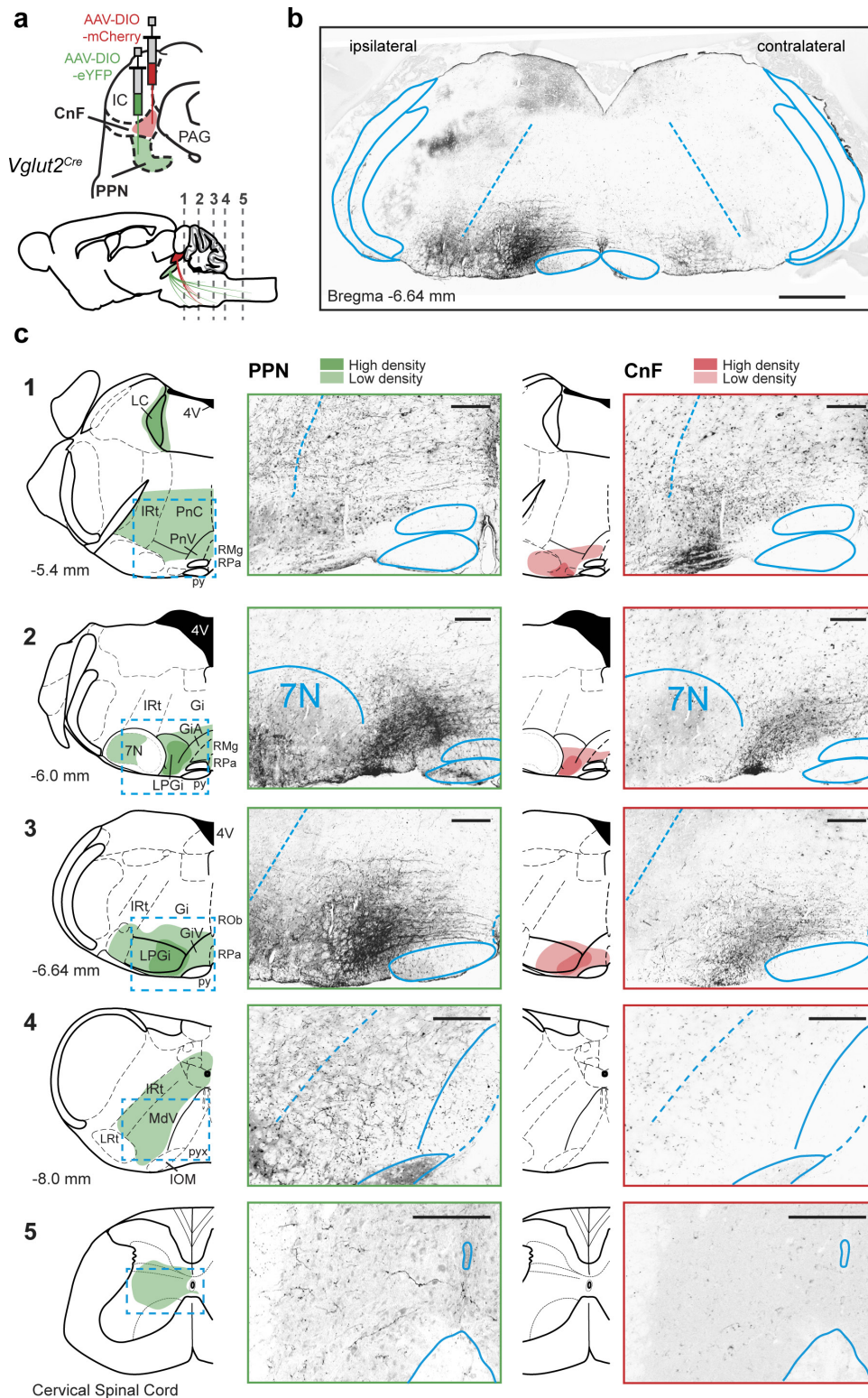
Extended Data Figure 7 | Summary of injection sites in the PPN and the CnF for hole-board stimulation experiments. **a**, Expression of ChR2 and fibre-tip positions in the CnF (left) or the PPN (right) for mice used in the

experiments shown in Fig. 5d, e. The mouse brain schematics in this figure have been reproduced with permission from Elsevier³⁸.



Extended Data Figure 8 | Connectivity between the PPN and the CnF. **a, b,** AAV-EF1a-FLEX-GTB helper virus followed by EnvA G-deleted-rabies-mCherry virus were unilaterally injected in the PPN (left, red) or the CnF (right, blue) in *Vglut2^{cre}* mice to trace inputs to glutamatergic neurons. Schematics summarizing the inputs to Vglut2⁺PPN neurons

(red) and Vglut2⁺CnF neurons (blue) are shown in **a**; the thickness of the arrows indicates the amount of connectivity based on the counts of the normalized number of neurons as shown in **b**. Dashed arrows indicate sparse connectivity.



Extended Data Figure 9 | The CnF and PPN have different descending output matrices. **a**, Simultaneous unilateral injection (top) of AAV-DIO-ChR2 virus in the CnF (mCherry, red) and the PPN (eYFP, green) in *Vglut2^{Cre}* mice ($N = 3$). Sagittal view of the brain (bottom) displaying the location in the brainstem (1–4) and the spinal cord (5) of the coronal sections shown in **c**. **b**, Coronal section showing ipsilateral and contralateral projection areas from glutamatergic PPN neurons and contralateral projection areas from glutamatergic PPN neurons. **c1–5**, Schematics and coronal sections showing projection areas from glutamatergic PPN (left, green) and CnF (right, red) neurons onto nuclei in the pons, medulla and spinal cord. In the schematics, the darker shades delineate the areas with the highest density of projections. In coronal sections, labelled processes are seen in black. Anatomical landmarks are

indicated in the schematics. Scale bars, 200 μm . 4V, fourth ventricle; 7N, facial motor nucleus; Gi, gigantocellular nucleus; GiA, gigantocellular reticular nucleus, alpha part; GiV, gigantocellular reticular nucleus, ventral part; IOM, inferior olive, medial nucleus; IRT, intermediate reticular nucleus; LC, locus coeruleus; LPGi, lateral paragigantocellular nucleus; LRT, lateral reticular nucleus; MdV, medullary reticular nucleus, ventral part; PnC, pontine nucleus, caudal part; PnV, pontine reticular nucleus, ventral part; pyx, pyramidal decussation; RMg, raphe magnus; ROb, raphe obscurus; RPa, raphe pallidus. The mouse brain schematics in this figure have been reproduced with permission from Elsevier³⁸.

Life Sciences Reporting Summary

Nature Research wishes to improve the reproducibility of the work that we publish. This form is intended for publication with all accepted life science papers and provides structure for consistency and transparency in reporting. Every life science submission will use this form; some list items might not apply to an individual manuscript, but all fields must be completed for clarity.

For further information on the points included in this form, see [Reporting Life Sciences Research](#). For further information on Nature Research policies, including our [data availability policy](#), see [Authors & Referees](#) and the [Editorial Policy Checklist](#).

► Experimental design

1. Sample size

Describe how sample size was determined.

The same sample size is typically used in the literature.

2. Data exclusions

Describe any data exclusions.

Only animals that got unhealthy or where viral injections were not correctly targeted were excluded from the study.

3. Replication

Describe whether the experimental findings were reliably reproduced.

In most of the experiments several trials were performed.

4. Randomization

Describe how samples/organisms/participants were allocated into experimental groups.

Randomization was not applied.

5. Blinding

Describe whether the investigators were blinded to group allocation during data collection and/or analysis.

Investigators were not blinded except for experiments in Figure 5.

Note: all studies involving animals and/or human research participants must disclose whether blinding and randomization were used.

6. Statistical parameters

For all figures and tables that use statistical methods, confirm that the following items are present in relevant figure legends (or in the Methods section if additional space is needed).

n/a | Confirmed

- The exact sample size (n) for each experimental group/condition, given as a discrete number and unit of measurement (animals, litters, cultures, etc.)
- A description of how samples were collected, noting whether measurements were taken from distinct samples or whether the same sample was measured repeatedly
- A statement indicating how many times each experiment was replicated
- The statistical test(s) used and whether they are one- or two-sided (note: only common tests should be described solely by name; more complex techniques should be described in the Methods section)
- A description of any assumptions or corrections, such as an adjustment for multiple comparisons
- The test results (e.g. P values) given as exact values whenever possible and with confidence intervals noted
- A clear description of statistics including central tendency (e.g. median, mean) and variation (e.g. standard deviation, interquartile range)
- Clearly defined error bars

See the web collection on [statistics for biologists](#) for further resources and guidance.

► Software

Policy information about [availability of computer code](#)

7. Software

Describe the software used to analyze the data in this study.

Reference to computer code publicly available is reported in the methods section. Ad hoc scripts have been developed for analysis purposes (described in the methods section). Those scripts are not publicly available but can be provided from the corresponding authors upon reasonable request.

For manuscripts utilizing custom algorithms or software that are central to the paper but not yet described in the published literature, software must be made available to editors and reviewers upon request. We strongly encourage code deposition in a community repository (e.g. GitHub). *Nature Methods* [guidance for providing algorithms and software for publication](#) provides further information on this topic.

► Materials and reagents

Policy information about [availability of materials](#)

8. Materials availability

Indicate whether there are restrictions on availability of unique materials or if these materials are only available for distribution by a for-profit company.

N/A

9. Antibodies

Describe the antibodies used and how they were validated for use in the system under study (i.e. assay and species).

Reference to all antibodies used are given in methods section.

10. Eukaryotic cell lines

a. State the source of each eukaryotic cell line used.

N/A

b. Describe the method of cell line authentication used.

N/A

c. Report whether the cell lines were tested for mycoplasma contamination.

N/A

d. If any of the cell lines used are listed in the database of commonly misidentified cell lines maintained by [ICLAC](#), provide a scientific rationale for their use.

N/A

► Animals and human research participants

Policy information about [studies involving animals](#); when reporting animal research, follow the [ARRIVE guidelines](#)

11. Description of research animals

Provide details on animals and/or animal-derived materials used in the study.

Strains, sex and age of animals are reported in methods section.

Policy information about [studies involving human research participants](#)

12. Description of human research participants

Describe the covariate-relevant population characteristics of the human research participants.

N/A